Magnetically textured γ-Fe[sub 2]O[sub 3] nanoparticles in a silica gel matrix: Optical and magneto-optical properties

F. Bentivegna, M. Nyvlt, J. Ferré, J. P. Jamet, A. Brun, S. Višňovsky, R. Urban

Magnetically textured γ-Fe_2O_3 nanoparticles in a silica gel matrix: Optical and magneto-optical properties

F. Bentivegna[a)]
Institut d'Optique Théorique et Appliquée, URA CNRS 14, Bât. 503, Université Paris XI, 91405 Orsay, France

M. Nyvlt
Institute of Physics, Charles University, Ke Karlovu 5, 12116 Praha 2, Czech Republic

J. Ferré[b)] and J. P. Jamet
Laboratoire de Physique des Solides, URA CNRS 2, Bât. 510, Université Paris XI, 91405 Orsay, France

A. Brun
Institut d'Optique Théorique et Appliquée, URA CNRS 14, Bât. 503, Université Paris XI, 91405 Orsay, France

Š. Višňovsky and R. Urban
Institute of Physics, Charles University, Ke Karlovu 5, 12116 Praha 2, Czech Republic

(Received 10 June 1998; accepted for publication 5 November 1998)

Optical and magneto-optical properties of maghemite superparamagnetic particles dispersed ($f=0.28$ vol % γ-Fe_2O_3) in a silica gel matrix have been studied at room temperature in the 1.5–3.7 eV spectral range. A permanent optical anisotropy can be induced when applying a magnetic field during the sol-gel freezing process. The permanent linear dichroism and birefringence in such in-plane magnetically textured samples are attentively studied. The spectral dispersion of Faraday effects in our textured samples is analyzed taking into account the in-plane optical anisotropy. Such a composite material is a promising candidate for future magneto-optical applications. © *1999 American Institute of Physics.* [S0021-8979(99)00404-1]

I. INTRODUCTION

Nanoscopic materials are the subject of intense current research. In particular, physical and chemical properties of nanophase composite materials can differ from their bulk counterparts, especially because of the major role played by surface effects and due to the electronic confinement at these extremely small dimensions.[1,2] Among them, nanocomposite materials including magnetic particles are very interesting for applications since they exhibit new exciting electronic, magnetic, and optical properties.[3–5]

It is now possible to prepare dispersed superparamagnetic particles with calibrated size in transparent matrices which give rise to interesting magnetic and optical properties.[3,6] Such composite materials containing particles smaller than the wavelength of light open the possibility to produce well adapted new magneto-optic media[7,8] which may surpass bulk or thin film materials. In particular, they combine good adaptable transparency and large magneto-optical effects at room temperature.[9] These compounds are promising candidates for applications involving optoelectronic devices based on magnetic and magneto-optic principles, such as optical fiber sensors[10] and optical isolators.[11,12]

Up to now only a few experimental works have been devoted to such nanocomposite magnetic materials.[6,13–17] A good way to stabilize assemblies of isolated magnetic particles is to embed them in transparent silica gel matrices.[17] Such magnetically textured systems, composed of oriented superparamagnetic particles frozen in glass-like matrices, are promising for future magneto-optical applications. In such media, a magnetic texture can be induced under a preparation magnetic field $\mathbf{B}_p$ applied during the sol-gel freezing process. A large permanent optical linear birefringence has been recently evidenced in the textured medium of magnetically oriented γ-Fe_2O_3 particles embedded in a silica gel matrix.[14] This stands as a direct proof that the frozen superparamagnetic particles are locked along their individual anisotropy axes in the gel matrix.

The preparation method and the structural and magnetic properties of the presently studied γ-Fe_2O_3 maghemite nanocomposite glasses have been reported in detail by the authors in the previous paper.[17] The structure and hardness of the silica-based matrix are close to those of usual glass. Silica gel matrices are also highly transparent in the visible spectral range. Transmission electron microscopy confirmed that the particles have only a very small ellipticity. Thus, in first approximation they can be considered spherical with a diameter D distributed according to a log-normal density function with a mean value $D_m=(10.5\pm1.1)$ nm and a standard deviation $\sigma=(4.6\pm0.6)$ nm. The particles are well separated from each other, which reduces their dipolar coupling to a

a)Present address: Research Institute for Materials, Spectroscopy of Solids and Surfaces, University of Nijmegen, Toernooiveld 1, 6525 ED-Nijmegen, The Netherlands.
b)Corresponding author; electronic mail: ferre@lps.u-psud.fr

negligible level at the considered low volumic fraction of particles, $f=0.28\%$

In the previous paper,[17] three types of samples, named "N," "O," and "T," were studied. For the type N specimens, the gel was solidified in the absence of any magnetic field in order to generate an isotropic distribution of the easy anisotropy axes of the particles. For the type O (respectively type I) specimens, the preparation field B_p was applied along the z axis (resp. perpendicular to z), i.e., normal to the plane (resp. in the plane) of the sample platelet. The effect of the magnetic texture on the in-field magnetization curves was investigated and compared with the corresponding behaviour of the type N nontextured sample and of the ferrofluid solution itself.[17] These data were well interpreted in the frame of the Raikher theory[18] extended to a polydisperse case, i.e., by taking into account the distribution of particle diameters. As expected for all first-order magnetooptical effects we proved that, at least, the Faraday ellipticity was proportional to the sample magnetization within the experimental error in the considered field range.[17]

This second article reports on optical and magnetooptical properties of such γ-Fe_2O_3 maghemite superparamagnetic particles dispersed in a xerogel matrix. In Sec. II, the two magnetooptical arrangements used in this study will be briefly described. The optical and magnetooptical effects in type N and O samples will be discussed first in Sec. III, before investigating in Secs. IV and V, the consequence of a preparation field B_p inducing an in-plane texture in type I samples. The induced optical anisotropy (linear dichroism and birefringence) and magnetooptical effects of the first (Faraday rotation and magnetic circular dichroism) or second order (magnetic linear dichroism and birefringence) in magnetization will be discussed, as well as their photon energy dispersion spectra. The structural, magnetic, and field induced contributions to the linear dichroism and birefringence will be compared.

II. EXPERIMENTAL TECHNIQUES

Optical and magneto-optical effects have been widely used to measure the magnetization and magnetic anisotropy in ferrofluids.[19,20] We shall report on room temperature optical measurements of the texture induced optical anisotropy by linear birefringence (LB) and linear dichroism (LD), and on magneto-optical studies of Faraday rotation (FR) and ellipticity (FE). The field induced magnetic linear birefringence (MLB) and dichroism (MLD) will be also briefly discussed.

For the studies of LB, LD, and magnetooptical effects, two ellipsometers were used. The first one, working at a fixed laser wavelength, has allowed measurements of these effects as a function of the applied magnetic field, and the study of the angular dependence of the LB and LD with respect to the texture orientation. The second apparatus was used for spectroscopic studies, i.e., to determine the variation of these effects with photon energy.

Polarization properties of the sample in light transmission along the z axis can be, in general, characterized by the Jones Cartesian transmission matrix relating the electric field amplitudes of incident (i) and transmitted (t) linearly polarized waves in the xy plane:

$$\begin{bmatrix} E_x^{(t)} \\ E_y^{(t)} \end{bmatrix} = \begin{bmatrix} t_{xx} & t_{xy} \\ t_{yx} & t_{yy} \end{bmatrix} \begin{bmatrix} E_x^{(i)} \\ E_y^{(i)} \end{bmatrix}. \tag{1}$$

Magneto-optical observables are related to the complex ratio t_{yx}/t_{xx} between the off-diagonal and diagonal elements of the Jones transmission matrix. The ellipsometers used for studying magneto-optical effects in light transmission measure, in most cases, the real and imaginary parts of this ratio.

Details on the first magneto-optical arrangement, which was in this case operating with a green HeNe laser light source ($\lambda \cong 543$ nm), have been described previously.[21,22] Sensitive measurements based on the modulation of the state of polarization of light are performed through a lock-in detection technique at high frequency $\nu = 50$ kHz. In polar configuration (with field B applied along the light propagation direction z), the magnetic circular dichroism or Faraday ellipticity (FE) is measured at the frequency ν while Faraday rotation (FR) is detected at 2ν. In the transverse (or Voigt–Cotton–Mouton) configuration (with B perpendicular to z), LD and MLD are detected at 2ν, while LB and MLB polarimetric measurements are performed at the frequency ν. As will be shown later, azimuthal LD and LB studies allow the determination of the easy direction of the magnetic anisotropy axes in textured samples.

The spectroscopic arrangement is based on a compensation technique using an azimuthal modulation of the light polarization by a Faraday cell.[22,23] The optical configuration is: Xe arc lamp—monochromator—polarizer—Faraday compensation and modulation cells—sample—analyzer—photomultiplier. The measured signal is proportional to the angle of compensation which is determined by the amplitude of the photoelectric current at the modulation frequency (2 kHz), at nearly saturated feedback. This signal provides FR or LD quantities. In order to get FE, a calibrated phase retarder is inserted between the modulation cell and the sample. The investigated photon energy range is 1.25–5.60 eV with a resolution of about 0.02 eV. For the considered samples, with typical thickness of a fraction of a millimeter, the upper energy part of the spectra was limited by the absorption edge of γ-Fe_2O_3.

III. OPTICS AND MAGNETO-OPTICS IN SAMPLES WITHOUT IN-PLANE MAGNETIC TEXTURE

This section is devoted to type N specimens, prepared without applying any magnetic field, and type O specimens which are examined optically or magneto-optically with light propagating along the z axis, i.e., along the favoured magnetization direction. Under these conditions there is no optical anisotropy in the plane of the platelet.

A. The dielectric tensor

The general form of the relative permittivity tensor is determined by the symmetry of the physical system. Let us first consider the case of a nontextured type N sample. When a magnetic field B is applied along the z axis, i.e., perpen-

dicular to the plane of the platelet, the complex effective permittivity tensor for our studied composite media should obey the symmetry C_∞ and is written:

$$\epsilon = \begin{bmatrix} \epsilon_{xx} & \epsilon_{xy} & 0 \\ \epsilon_{yx} & \epsilon_{yy} & 0 \\ 0 & 0 & \epsilon_{zz} \end{bmatrix}, \tag{2}$$

where the ϵ_{ij} components depend on B. When $B=0$, one has $\epsilon_{xx}=\epsilon_{yy}=\epsilon_{zz}$ and $\epsilon_{xy}=\epsilon_{yx}=0$. When $B\neq 0$, the relations $\epsilon_{xx}=\epsilon_{yy}\neq\epsilon_{zz}$ and $\epsilon_{yx}=-\epsilon_{xy}$ hold.

For a type O sample, solidified under a preparation field B_p applied along the z axis, the symmetry C_∞ is not affected. Thus the tensor form (2) remains valid, except that ϵ_{zz} differs from $\epsilon_{xx}=\epsilon_{yy}$ even if $B=0$, due to the texture induced by B_p.

Since the size of the embedded magnetic particles is far smaller than the optical wavelength (i.e., the electromagnetic field changes only slightly on a scale comparable with the characteristic particle size), the ϵ_{ij} components of the composite medium can be calculated from the effective dielectric theory.[24,25]

The optical and magnetooptical spectra of maghemite γ-Fe_2O_3 nanoparticles, embedded in a nonmagnetic, amorphous, glass-like host matrix depend both on the complex dielectric constant ϵ_g of glass and on the components of the complex dielectric tensor ϵ_m of γ-Fe_2O_3. These spectra may differ significantly from those displayed by γ-Fe_2O_3 continuous films. As a matter of fact, the ϵ_{ij} components of the effective dielectric tensor (2) of the composite are functions of the components of the ϵ_m tensor and of ϵ_g, of the form factor (i.e., the ratio between the long and short axes of the particles which are assumed to be ellipsoids) and of the volumic fraction f of the particles.[24]

B. Optical absorption

The absorption coefficient α, characterizing the exponential decay of the light intensity during propagation along z in the nontextured composite material is given by:

$$\alpha = \frac{4\pi}{\lambda} \mathrm{Im}\sqrt{\epsilon_{xx}}, \tag{3}$$

where Im means the imaginary part of the following quantity (i.e., the extinction coefficient). The absorption coefficient α_m of a γ-Fe_2O_3 film ($f=1$) is obviously obtained considering ϵ_{xx} for the bulk material. In contrast, the absorption coefficient α of the composite material depends at the very least on the real refractive index of glass, even if one assumes a transparent glass-like matrix. Therefore, the ratio $\alpha/f\alpha_m$ differs in general from unity.

Since the magnetically induced variations of the optical indices are far smaller than unity, the optical transmission spectra of our type N or O samples are close to those obtained for the type I sample (Fig. 1). The absorption edge manifests itself as a strong increase of the absorption coefficient α around 3.2 eV (Fig. 2). The small absorption bump around 2.5 eV can be assigned to Fe^{3+} optical transitions (see Sec. III C).

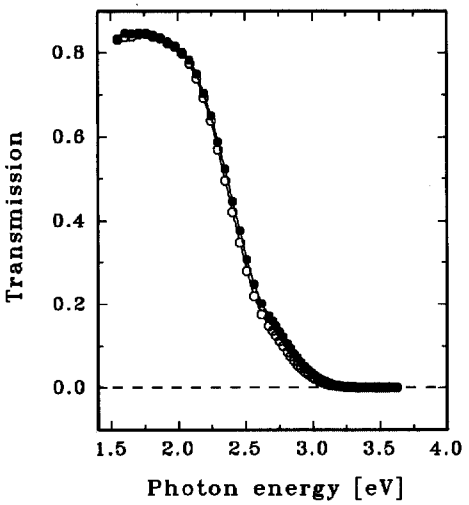

FIG. 1. Optical transmission spectra for a type I sample, for light polarized parallel (empty circles) or perpendicular (full circles) to the preparation field (B_p) direction. Sample thickness: $d=0.275$ mm.

Let us now compare first the effective (α/f) absorption spectrum of, for example, our sample N with those obtained for γ-Fe_2O_3 particles frozen in a polymer matrix, reported by Ziolo *et al.*[3] and Vassiliou *et al.*[26] normalized by their corresponding volumic fraction f. These authors compared the absorption spectrum of the composite material with that of a thick γ-Fe_2O_3 film. Surprisingly, the absorption edge of the nanocomposite was redshifted with respect to that of bulk γ-Fe_2O_3 (Fig. 2). They attributed this effect to an existence of lattice strains in small particles.[26] In our compound we instead observe a blueshift of the edge when the absorption curve is compared to the bulk data reported by Ziolo *et al.*,[3] but a smaller shift is detected with respect to the results in a γ-Fe_2O_3 film reported by Wang *et al.*[27] (especially if one takes into account the discussion presented at the beginning

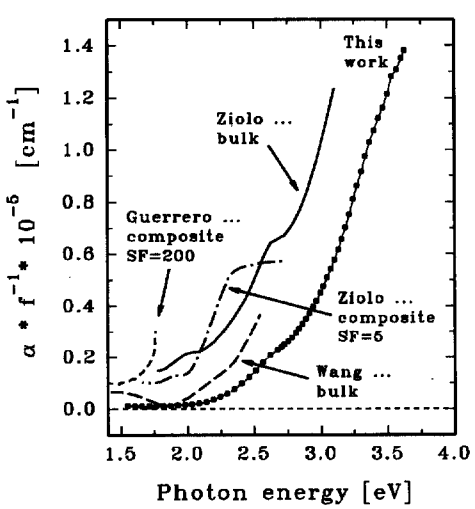

FIG. 2. Effective optical absorption (i.e., the quantity α/f) spectrum for the type N sample (points) compared with absorption spectra of γ-Fe_2O_3 particles frozen in a SiO_2 matrix (Ref. 9) (short dashes), of γ-Fe_2O_3 particles in a polymer matrix (Ref. 3) (dash-dot line) and of thin γ-Fe_2O_3 films, epitaxially grown (Ref. 3) by halide decomposition (Ref. 31) (solid line) or by sputtering (Ref. 27) (long dashes). Note the SF scaling factors used to distinguish between different absorption curves.

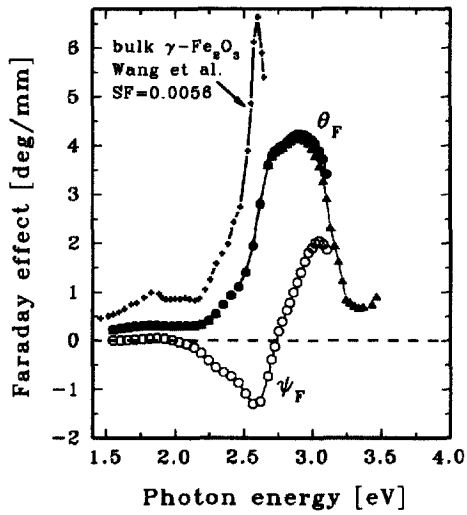

FIG. 3. Specific Faraday rotation (full circles and triangles) and ellipticity (empty circles) for a type O sample at $B=0.18$ T. Sample thicknesses were $d=0.275$ mm (circles) and 0.310 mm (triangles). The specific Faraday rotation spectrum of a sputtered thin γ-Fe_2O_3 film (Ref. 27) (small crosses), was multiplied by a SF factor equal to $2/f$ (f of our sample) in order to separate the two Faraday curves.

of this section). Guerrero *et al.*[9] have also reported recently on the absorption spectrum of a highly concentrated γ-Fe_2O_3/SiO_2 nanocomposite between 1.46 and 1.76 eV, but this spectral range is too narrow for an extended comparison.

C. Magneto-optical effects

The complex Faraday effect Φ_F in type N or O samples having a thickness d, measured for light propagating along the z axis (normal to the platelet), is expressed by the usual formula:

$$\Phi_F=\theta_F-i\psi_F=\frac{2\pi}{\lambda}\Delta N_F^0 d=i\pi\frac{d}{\lambda}\frac{\epsilon_{xy}}{\sqrt{\epsilon_{xx}}}. \tag{4}$$

for small values of the Faraday rotation θ_F and ellipticity ψ_F angles, as justified in our case. As for the absorption, the ratios $\theta_F/f\theta_{Fm}$ and $\psi_F/f\psi_{Fm}$ will in general differ from unity (the subscript m still refers to the γ-Fe_2O_3 bulk material).

The Faraday rotation (FR) and ellipticity (FE) spectra, measured at $B=0.18$ T, for light propagating along the z axis, are shown in Fig. 3. The variation of the first-order magneto-optical effects in an applied field B depends obviously on the degree of particle orientation along z induced by B_p during the freezing process in the same way as the corresponding magnetization.[17] Precisely speaking, the particles are fixed in the matrix, so that the magnetization process only involves the so-called Néel rotation of the magnetic moments inside the particles.

Whereas the FR and FE signals are weak below 2.2 eV (Fig. 3), their magnitude increases at the front edge of the γ-Fe_2O_3 absorption band (Fig. 2). Note that the FE changes sign around 2.75 eV. This comes from the presence of, at least, two absorption components, located near 2.6 and 3 eV, which are also revealed as shoulders in the optical absorption spectrum (Fig. 2). These FR and FE spectra are very comparable in shape to those exhibited by $Y_3Fe_5O_{12}$, another magnetic material containing ferric ions (Fig. 5 of Ref. 28), but they are indeed less structured than in this single crystal. Since the values of θ_F or ψ_F do not differ more than by a factor of 2 between our sample and $Y_3Fe_5O_{12}$, we may assign the absorption bands located in the 2.4–3.1 eV region in our sample to electric dipolar exchange induced $3d^5(^6A_{1g}) \rightarrow 3d^4s(^4T_{2g},^4E_g,^4A_{1g})$ transitions of the Fe^{3+} ions in octahedral sites.[28,29]

Note that our specific FR data, renormalized by f, are consistent with those measured by Guerrero *et al.*,[9] over the $1.46<E<1.76$ eV range, on a γ-Fe_2O_3/SiO_2 composite material. Moreover, the shape of the specific FR spectrum in thin sputtered films of γ-Fe_2O_3, as reported by Wang *et al.*[27] in the $1.42<E<2.60$ eV range, is in good agreement with our data (Fig. 3), especially if one compares the factor of merit in both cases, i.e., the effective FR divided by the absorption coefficient α. Note that the measurement of Faraday dispersion at energies higher than 3.2 eV becomes difficult due to a very strong optical absorption.

A large enhancement of the first-order magneto-optical effects is also expected near the surface plasmon resonance of dispersed small spherical particles, due to a large increase of the local field at this particular frequency.[25] There is no way, however, in our case, to separate this contribution from the bulk part of the spectrum.

In the absence of magnetic field B, applied in the xy plane of the platelet, symmetry arguments forbid any optical anisotropy in the type N or O samples when the light propagates along z. When a magnetic field is applied inside the xy plane, second order magneto-optical effects [magnetic linear birefringence (MLB) and dichroism (MLD)] are observed. It has been already demonstrated that, as expected for fixed particles, these effects vary as the square of the magnetization $M^2(B)$ (Fig. 7 of Ref. 17).

IV. OPTICAL AND MAGNETO-OPTICAL EFFECTS IN SAMPLES WITH IN-PLANE MAGNETIC TEXTURE

A. Electromagnetic waves in a uniaxial magnetized medium

We shall now develop a general analysis of the electromagnetic wave propagation in a platelet with an in-plane optical anisotropy axis, under a magnetic field B applied perpendicularly to the plane. Then, we shall discuss the optical birefringence and dichroism. Finally we will analyze the complex Faraday effect in our specimens in the presence of the induced in-plane optical anisotropy.

For the following calculations it is convenient to introduce two cartesian referentials (Fig. 4): xyz, associated to light, and XYZ, related to the sample, with identical z and Z axes perpendicular to the plane of the platelet and parallel to the light wave vector. X is then defined as the magnetic in-plane anisotropy axis, i.e., along the preparation field B_p applied during the freezing process, so that X makes an angle φ with respect to x.

Under a field $B\|z$, the complex components of the dielectric tensor (1) are written as

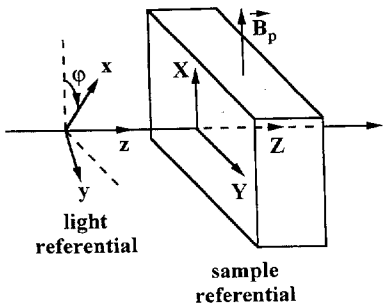

FIG. 4. Relative Cartesian referentials, *xyz* for light and *XYZ* for the sample (the light wave propagates along $z\|Z$). The magnetic preparation field B_p was applied along X during the freezing procedure.

$$\epsilon_{xx}=\epsilon_0+\epsilon_2\cos 2\varphi, \quad \epsilon_{yy}=\epsilon_0-\epsilon_2\cos 2\varphi,$$
$$\epsilon_{xy}=-i\epsilon_1+\epsilon_2\sin 2\varphi, \quad \epsilon_{yx}=i\epsilon_1+\epsilon_2\sin 2\varphi. \tag{5}$$

Here, ϵ_1, responsible for the magneto-optical activity, is proportional to the magnetization (we neglect here higher order terms), while ϵ_2 represents the in-plane optical anisotropy. Starting from the eigenvalue equation for the complex refractive indices $N_\pm$, characterizing the propagation of the four eigenmodes,[30] one deduces

$$\begin{aligned} N_\pm^2&=(n_\pm-ik_\pm)^2\\ &=\tfrac{1}{2}\{(\epsilon_{xx}+\epsilon_{yy})\pm[(\epsilon_{xx}-\epsilon_{yy})^2+4\epsilon_{xy}\epsilon_{yx}]^{1/2}\}\\ &=\epsilon_0\pm(\epsilon_1^2+\epsilon_2^2)^{1/2}. \end{aligned} \tag{6}$$

The eigenmodes can be expressed by their electric field vectors:

$$\begin{aligned} \mathbf{E_1}&=\begin{bmatrix}\delta\\ \epsilon_{yx}\end{bmatrix}\exp\left[i\left(\omega t-\frac{2\pi}{\lambda}N_+z\right)\right],\\ \mathbf{E_2}&=\begin{bmatrix}\delta\\ \epsilon_{yx}\end{bmatrix}\exp\left[i\left(\omega t+\frac{2\pi}{\lambda}N_+z\right)\right],\\ \mathbf{E_3}&=\begin{bmatrix}\epsilon_{xy}\\ -\delta\end{bmatrix}\exp\left[i\left(\omega t-\frac{2\pi}{\lambda}N_-z\right)\right],\\ \mathbf{E_4}&=\begin{bmatrix}\epsilon_{xy}\\ -\delta\end{bmatrix}\exp\left[i\left(\omega t+\frac{2\pi}{\lambda}N_-z\right)\right], \end{aligned} \tag{7}$$

where

$$\begin{aligned} \delta&=\tfrac{1}{2}\{(\epsilon_{xx}-\epsilon_{yy})+[(\epsilon_{xx}-\epsilon_{yy})^2+4\epsilon_{xy}\epsilon_{yx}]^{1/2}\}\\ &=(\epsilon_1^2+\epsilon_2^2)^{1/2}+\epsilon_2\cos 2\varphi. \end{aligned} \tag{8}$$

In the limiting case $\epsilon_2=0$, the eigenmode polarizations are circular and the sample exhibits a pure Faraday effect, as described in the previous section. On the other hand, when $\epsilon_1=0$, the eigenmodes are linearly polarized and the sample behaves as a phase plate. This latter case will now be treated.

B. Optical anisotropy: linear birefringence and dichroism

In this section, we shall consider the case of a type I sample, solidified in the presence of a preparation field B_p applied in the plane of the platelet along X. The in-plane induced magnetic texture gives rise to an optical anisotropy which can be detected through LB or LD measurements, for light propagating along the z axis, in the absence of any magnetic field. A strong permanent LB has already been evidenced in our magnetically textured γ-Fe_2O_3 gel samples.[14] The comparison between the magnitude of this LB and that found for a magnetically saturated ferrofluid with the same composition confirms the tendency of a spatial locking of the principal axes of the oriented γ-Fe_2O_3 particles towards the preparation field direction. In the present type I samples, the optical anisotropy is large enough to affect significantly the optical transmission (Fig. 1).

Let us now complete the analysis developed in the previous section in the special case where $\epsilon_1=0$. The expression (8) then provides $\delta=2\epsilon_2\cos^2\varphi$ and from Eq. (7) one can immediately deduce that the eigenmodes $\mathbf{E_1}$ and $\mathbf{E_2}$ ($\mathbf{E_3}$ and $\mathbf{E_4}$) are linearly polarized along $X(Y)$ axis, their propagation being characterized by the refractive index $N_+(N_-)$. The LB and LD quantities are respectively related to the real, $\Delta n_L^0=(n_+-n_-)/2$, and imaginary, $\Delta k_L^0=(k_+-k_-)/2$, parts of the complex linear birefringence $\Delta N_L^0=(N_+-N_-)/2$. Using expression (6) and assuming $|\epsilon_2|\ll|\epsilon_0|$, one obtains

$$\Delta N_L^0\approx\frac{\epsilon_2}{2\sqrt{\epsilon_0}}. \tag{9}$$

When treating the optical configuration we have already mentioned in Sec. II that magnetooptical ellipsometers measure, in most cases, the complex ratio t_{yx}/t_{xx} of the off-diagonal to diagonal elements of the transmission Cartesian Jones matrix (1). For originally isotropic media it measures the complex Faraday (Φ_F) effect. For magnetically textured samples, it will be shown that this ratio Φ is now related to the in-plane optical anisotropy of the specimen.

The values of t_{yx} and t_{xx} follow from boundary conditions for electromagnetic fields at front and rear interfaces of the platelet.[30] Because the samples exhibit significant absorption, it is realistic to restrict ourselves to propagation effects and neglect the reflections at the interfaces. Then

$$\frac{t_{yx}}{t_{xx}}=\Phi=\frac{-i\epsilon_2\sin 2\varphi\tan[(2\pi/\lambda)\Delta N_L^0 d]}{\epsilon_2-i\epsilon_2\tan[(2\pi/\lambda)\Delta N_L^0 d]\cos 2\varphi}. \tag{10}$$

Since $|\epsilon_2|\ll|\epsilon_0|$, one can use Eq. (9) and neglect the second term ($\sim\epsilon_2^2$) in the denominator of Eq. (10). Moreover, one can approximate $\tan[(2\pi/\lambda)\Delta N_L^0 d]$ as $[(2\pi/\lambda)\Delta N_L^0 d]$ in our case. Then

$$\Phi\cong-i\frac{2\pi}{\lambda}\Delta N_L^0 d\sin 2\varphi=-i\frac{2\pi}{\lambda}\Delta N_L d. \tag{11}$$

Here the imaginary number i means that the LD signal is measured in the same way as FR while LB is detected as FE.

The azimuthal dependence with $\varphi=(X,x)$ (Fig. 5) predicted by Eq. (11) can be verified experimentally by measuring LB, Δn_L, and LD, Δk_L, signals when rotating the platelet around the z axis (Fig. 5). The extrema are well displayed for $\varphi=\pi/4+k\pi/2$. This can be easily understood if one considers an incident wave linearly polarized along x. For such critical values of φ, its magnitude will be equally distributed between two eigenmodes polarized along X and Y and thus the change of its polarization state will be maximized. On the

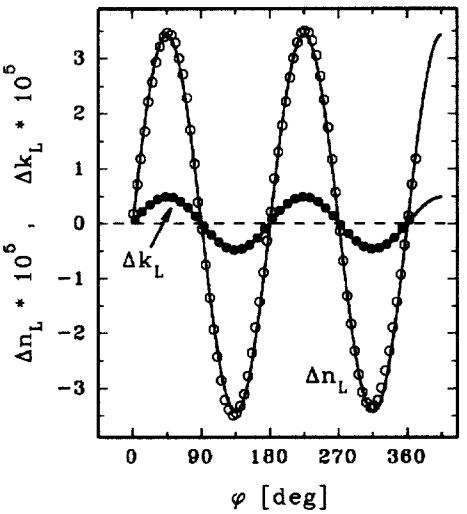

FIG. 5. Variation of Δn_L (empty circles) and Δk_L (full circles) with $\varphi=(X,x)$, measured at 2.28 eV on a type I sample (thickness: $d=0.374$ mm). The solid curves show the theoretical angular dependences given by Eq. (11).

other hand, for $\varphi=0+k\pi/2$ the incident linear polarization excites only one of the two eigenmodes. Thus, its polarization state remains unchanged and the corresponding signals are zero. Such kind of behavior is well known for a phase plate which is a nonabsorbing optical equivalent of the type I specimens. Ellipsometric experiments carried out at $\varphi \pm \pi/4$ provide values of the in-plane complex linear birefringence ΔN_L^0

$$\Delta N_L^0 \approx \frac{i\lambda}{4\pi d}[\Phi(\pi/4)-\Phi(-\pi/4)]. \tag{12}$$

C. Origin of the linear birefringence and dichroism

We wish first to discuss the origin of the LB and, second, to comment on the magnitude of Δn_L^0 which reflects the optical anisotropy of the system. In a non-frozen ferrofluid the particles are free to rotate in order to align their easy anisotropy axis along the direction of the applied field. Then, the LB comes from the optical anisotropy of the γ-Fe_2O_3 particles themselves. It can have a magnetocrystalline origin,[19,31] possibly reinforced by a tetragonal ordering of vacancies in the particles[32] or come from the particle shape anisotropy.[33,34] Shape-induced birefringence is also displayed, for example, by an ordered array of elongated optically isotropic particles dispersed in a liquid.[35]

Starting from a polydisperse ferrofluid solution, in the low concentration limit ($f \ll 1$), the real part of the birefringence of a gel frozen under a preparation field B_p is expressed as

$$\Delta n_L^0 = f\delta n_0 \int_0^\infty \left[1-\frac{3}{p_0\tanh(p_0)}+\frac{3}{p_0^2}\right]P(D)dD, \tag{13}$$

where $p_0=\mu(D)B_p/kT$ and $\mu(D)$ is the magnetic moment of a particle with diameter D. $P(D)$ stands for the distribution of D and δn_0 is the value of Δn_L^0 at magnetic saturation, extrapolated to $f=1$. The term in the square brackets of Eq. (13) can be called "degree of birefringence" for particles with diameter D. This quantity has been derived in Refs. 31, 33 and it is related to the degree of particle alignment. The whole integral over particle diameters then stands for the resultant degree of birefringence in an applied field B_p.

The origin of the LB in a textured sample is similar, but the degree of particle alignment decreases very slowly with time, which means that the particles can partly reorient themselves in their own environment because of ageing effects. For two diluted samples with $f=0.28\%$ and 0.14%, but prepared from the same ferrofluid batch, we verified that the LB is proportional to f, confirming our previous hypothesis of a single particle optical effect.

On the other hand, the field induced MLB or MLD in our samples arise from the spin rotation inside particles through the so-called Néel mechanism. These magnetic contributions, measured in the type N or I samples, are far smaller than the particle crystallographic and shape LB and LD contributions. For example, the MLD measured at 2.28 eV,[17] is two orders of magnitude smaller than the LD. As expected,[21] the MLB and MLD are nearly isotropic terms since they do not vary much with the rotation φ of the sample around z.

The single particle birefringence δn_0 can be deduced from the knowledge of Δn_L^0 and from the estimation of the degree of birefringence, related to the degree of particle alignment taking account of ageing effects. We found $\delta n_0 = 0.08$ at 2.28 eV, using the experimental value $\Delta n_L^0 = 3.5 \times 10^{-5}$ (Fig. 5) and a degree of birefringence equal to 0.16, as estimated from the experimental data.[17] This value of δn_0 is consistent with other previous estimations.[14,19]

D. Faraday effect measurements

For the in-plane magnetically textured sample I, the Faraday effect measurement is obviously perturbed by the permanent LB.[36,37] We shall now develop calculations for our absorbing system and show how it is possible to deduce the magnitude of this perturbation from the experimental data of the complex Faraday effect, linear birefringence and dichroism. This will be done for the whole photon energy spectra.

The calculation procedure is similar to that developed in Sec. IV A, but we are now dealing with general solutions derived from Eqs. (5) to (8), with $\epsilon_1 \neq 0$ and $\epsilon_2 \neq 0$.

When the reflections at the platelet interfaces are neglected, we obtain quite a simple expression for the measured complex signal Φ:

$$\frac{t_{yx}}{t_{xx}} \equiv \Phi = \frac{(\epsilon_1 - i\epsilon_2 \sin 2\varphi)\tan\left(\dfrac{\beta^+-\beta^-}{2}\right)}{(\epsilon_1^2+\epsilon_2^2)^{1/2} - i\epsilon_2 \tan\left(\dfrac{\beta^+-\beta^-}{2}\right)\cos 2\varphi} \tag{14}$$

with the propagation phase factors

$$\beta^{+(-)} = \frac{2\pi}{\lambda} N_{+(-)} d. \tag{15}$$

For a nonmagnetized sample ($\epsilon_1=0$), expression (14) becomes equivalent to Eq. (10). Therefore, the linear dichroism (birefringence) can be calculated from the real (imaginary) part of expression (12).

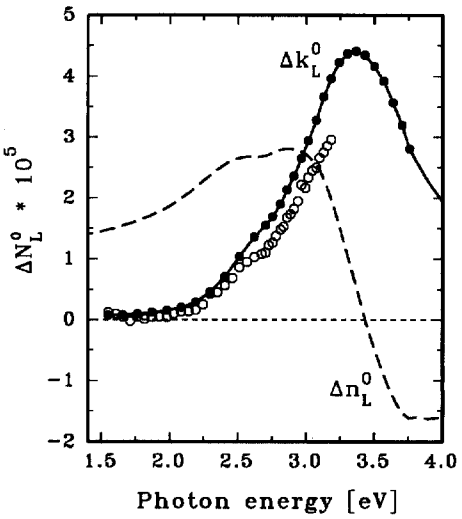

FIG. 6. Dispersion of the linear dichroism Δk_L^0 (full circles) and of the linear birefringence Δn_L^0 (dashed line) for the in-plane textured sample I. The linear dichroism Δk_L^0 spectrum (open circles), deduced from optical transmission data (Fig. 1), is included for comparison.

From experimental measurements of the real part of $[\Phi(\pi/4)-\Phi(-\pi/4)]$, the Δk_L^0 spectrum of the type I sample was deduced, as displayed in Fig. 6. Over the 1.5–3.2 eV photon energy range, it is consistent with that calculated directly from the transmission spectra for the two X and Y linear polarizations (Fig. 1). For practical reasons, we could not measure the linear birefringence Δn_L^0 spectrum of the sample. So, it was calculated from the knowledge of the Δk_L^0 spectrum using the Kramers–Kronig dispersion relationships (Fig. 6). It is worth mentioning that the value of Δn_L^0 at 2.28 eV is in reasonable agreement with our measurement by the ellipticity modulation technique (Fig. 5).

For $\varphi=k\pi$ or $\varphi=(2k+1)\pi/2$, with $k=0,1...$, the optical axis X of the sample is either parallel or perpendicular to the polarization axis x, and for these sample orientations a minimum of dc light intensity is detected. The values of the complex Faraday effect, $\Phi=\theta-i\psi$, obtained for $\varphi=0$ or $\pi/2$ are very different from each other. This is demonstrated experimentally both for Faraday rotation θ [Fig. 7(a)] and ellipticity ψ [Fig. 7(b)]. Now we shall try to explain these experimental data. Theoretically, such a difference $2\Delta\Phi$ can be evaluated from Eq. (14):

$$2\Delta\Phi=\Phi(0)-\Phi(\pi/2)=\frac{2i\epsilon_1\epsilon_2\tan^2\left(\frac{\beta^+-\beta^-}{2}\right)}{\epsilon_1^2+\epsilon_2^2\left[1+\tan^2\left(\frac{\beta^+-\beta^-}{2}\right)\right]}. \tag{16}$$

Under the condition $|\epsilon_1|\ll|\epsilon_2|\ll\epsilon_0$, which means that the optical properties of the material are not strongly modified and that the optical anisotropy perturbation dominates, we can write

$$\Delta\Phi=i\frac{\epsilon_1}{\epsilon_2}\sin^2\left(\frac{2\pi}{\lambda}\Delta N_L^0 d\right). \tag{17}$$

From Eq. (9) it is known that $\epsilon_2\approx 2\Delta N_L^0\sqrt{\epsilon_0}$ and similarly, $\epsilon_1\approx 2\ \Delta N_F^0\sqrt{\epsilon_0}$, where Δn_F^0 is the circular birefringence responsible for the intrinsic Faraday effect [this follows from Eq. (6) and it is consistent with Eq. (4)]. Substitution of ϵ_1 and ϵ_2 into Eq. (17) gives

$$\Delta\Phi\approx i\frac{\Delta N_F^0}{\Delta N_L^0}\sin^2\left(\frac{2\pi}{\lambda}\Delta N_L^0 d\right) \tag{18}$$

and when expecting that $|2\pi/\lambda\Delta N_L^0 d|\ll 1$, we finally get

$$\Delta\Phi=\Delta\theta-i\Delta\Psi\approx i\left(\frac{2\pi}{\lambda}\Delta N_F^0 d\right)\left(\frac{2\pi}{\lambda}\Delta N_L^0 d\right)\approx i\Phi_F\Phi_L. \tag{19}$$

This last equation shows that $\Delta\Phi$ is approximately proportional to the product of the average complex Faraday rotation $\Phi_F=[\Phi_F(0)+\Phi_F(\pi/2)]/2$ (standing here for intrinsic Faraday effect) by the complex linear birefringence $\Phi_L=[\Phi_L'-i\Phi_L'']$ with

$$\Phi_L'=\frac{2\pi}{\lambda}\Delta n_L^0 d \quad\text{and}\quad \Phi_L''=\frac{2\pi}{\lambda}\Delta k_L^0 d. \tag{20}$$

Compare with expressions (11) and (12), thus

$$\Delta\Phi=\Delta\theta-i\Delta\psi\approx i(\theta_F-i\psi_F)(\Phi_L'-i\Phi_L''). \tag{21}$$

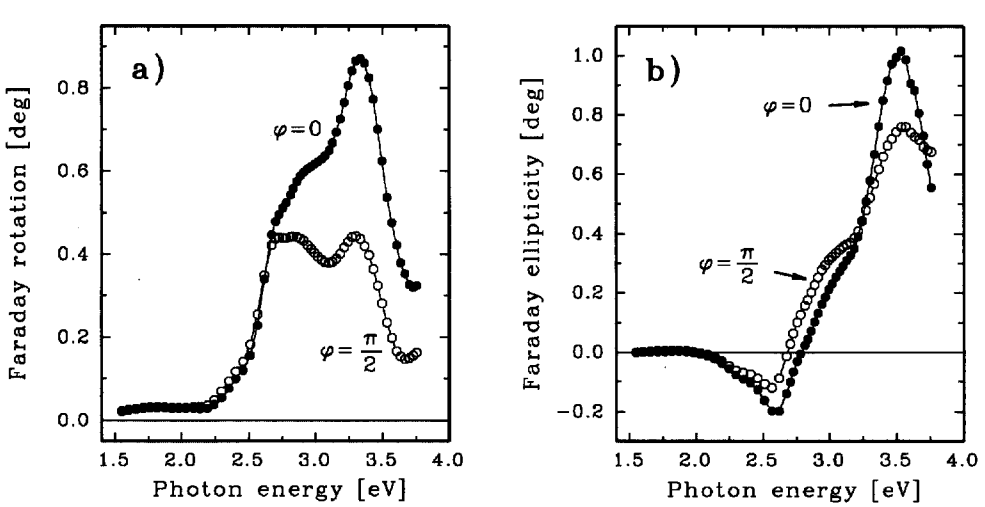

FIG. 7. (a) Faraday rotation and (b) ellipticity spectra measured at $B=0.18$ T, for two different azimuthal orientations $\varphi=0$ (full circles) and $\varphi=\pi/2$ (open circles) of the polarization with respect to the B_p direction in a magnetically textured type I sample (thickness $d=0.275$ mm).

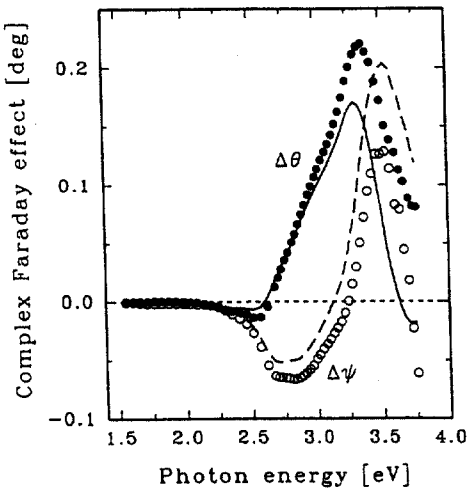

FIG. 8. Measured (circles) and calculated (lines) spectra of the change of the complex Faraday effect due to the in-plane optical anisotropy in a textured I sample. Experimental $\Delta\theta$ (full circles) or $\Delta\psi$ (empty circles) spectra are compared to those calculated using Eq. (22), from previously determined FR, FE, LB, and LD.

The separation of the real and imaginary parts of $\Delta\Phi$ leads to

$$\Delta\theta \approx \Phi'_L\psi_F + \Phi''_L\theta_F$$

$$\Delta\psi \approx -\Phi'_L\theta_F + \Phi''_L\psi_F . \qquad (22)$$

In Fig. 8 we plotted $\Delta\theta$ and $\Delta\psi$ as calculated from Eq. (22), making use of Δn_L^0 and Δk_L^0 (Fig. 6) and of the mean complex Faraday effect, obtained from experimental spectra shown in Fig. 7. These data are compared with the experimental differences: $\Delta\theta = [\theta(0) - \theta(\pi/2)]/2$ and $\Delta\psi = [\psi(0) - \psi(\pi/2)]/2$. Both experimental and theoretical results are in quite good agreement in spite of the approximation we used to obtain simplified expressions (18) and (19), and although the linear birefringence was calculated from the dichroism spectrum. Such a procedure could lead to large errors especially at high energies. This certainly explains why the discrepancy between the experiment and the theory becomes more significant above 3 eV.

The intrinsic Faraday spectra in sample I, i.e., the average of the dispersion curves shown in figure 7 for $\varphi = 0$ and $\varphi = \pi/2$, is reasonably close to that exhibited for the sample O (Fig. 3) except that a new spectroscopic structure appears above 3 eV in the former case. Up to now we have no explanation for this particular behavior.

V. CONCLUSION

We have reported on optical and magneto-optical properties of γ-Fe_2O_3 nanometric superparamagnetic particles frozen in silica-glass matrices over an extended spectral range. Contrarily to previous results on similar types of particles embedded in a polymer matrix,[3,26] we demonstrated that the absorption band edge is only slightly shifted as compared to that shown by a uniform thin film of γ-Fe_2O_3. At magnetic saturation and in the 1.5–2.6 eV spectral range, our nanocomposite material exhibits Faraday rotation of the same order of magnitude as $Y_3Fe_5O_{12}$, a compound widely used for magneto-optical applications.

A moderate (0.1 T) magnetic field B_p, applied in the plane of the sample platelet during the matrix solidification procedure, induces a large optical anisotropy. We obtain the so-called magnetically textured samples since the superparamagnetic particles orient themselves in such a way that their easy anisotropy axes are aligned towards B_p. The optical anisotropy related to the particle alignment is clearly detected by LB or LD when rotating the platelet around the light propagation axis. As expected, the LB or LD, arising from the bulk rotation of the particles during the sample preparation, are two orders of magnitude larger than the field induced magnetic linear birefringence or dichroism, which are due to Néel rotation of spins in frozen particles. The measured Faraday effects in such in-plane textured materials differ obviously from their original effects in their non-textured counterparts, because of their large permanent optical anisotropy. Faraday rotation and ellipticity data over the 1.5–3.7 eV spectral range are well fitted by our calculations, in spite of some crude simplifications.

Finally, we wish to emphasise some advantages of such nanocomposite magnetic materials frozen in an amorphous glass matrix:

(a) they can be prepared in large quantities and with easily controlled shapes at moderate prices,
(b) they show a large figure of merit in Faraday rotation which is close to that exhibited by YIG, an archetypal compound used for magneto-optical applications,
(c) Faraday rotation above 2.7 eV can be increased significantly in magnetically textured samples,
(d) one can induce a large optical anisotropy by magnetic texturation. This gives rise to a large linear birefringence ($\Delta n_L = 2\times10^{-5}$) in the red part of the spectrum where the sample is highly transparent.

All these interesting properties are very useful for applications such as optical rotators, isolators and modulators, based on magneto-optical principles. It is certainly possible to design high frequency magneto-optical devices with such materials since the dynamics is controlled by magnetisation switching time which could be smaller than 1 ns for a Néel spin rotation process.

ACKNOWLEDGMENTS

The authors wish to acknowledge F. Chaput and J. P. Boilot of the Laboratoire de Physique de la Matière Condensée of the Ecole Polytechnique, for all the samples they prepared by the sol-gel technique. They also thank D. Zins of the Laboratoire de Physico-Chimie de l'Université Pierre et Marie Curie for the ferrofluid preparation. One of the authors (M. N.) would like to express his thanks to the Solid State Optics group at Laboratoire de Physique des Solides, Université Paris-Sud for its kind hospitality, and the French Embassy in Prague for a financial support. This research was partly sponsored by the HCM programme "Magnetic properties of novel ultrathin films" (project No. ERBCIP-DCT940622). Partial support of Grant Agency of the Czech

Republic (GACR 202/97/1180) and Grant Agency of the Charles University (GAUK 43/198/B FYZ/MFF) is gratefully acknowledged.

[1] *Nanophase Materials: Synthesis, Properties, Applications*, edited by G. C. Hadjipanayis and R. W. Siegel, NATO ASI Ser. E, Applied Sciences (Kluwer, Dordrecht, 1994), Vol. 260.
[2] D. D. Awschalom and D. P. DiVincenzo, Phys. Today **48**, 43 (1995).
[3] R. F. Ziolo, E. P. Giannelis, B. A. Weinstein, M. P. O'Horo, B. N. Ganguly, V. Mehrotra, M. W. Russell, and D. R. Huffman, Science **257**, 219 (1992).
[4] L. E. Brus *et al.*, J. Mater. Res. **4**, 704 (1989).
[5] Science **254**, 1300 (1991).
[6] R. D. Shull, J. J. Ritter, A. J. Shapiro, L. J. Swartzendruber, and L. H. Bennett, J. Appl. Phys. **67**, 4490 (1990).
[7] L. Gunther, Phys. World **3**, 28 (1990).
[8] *Applied Magnetism*, edited by R. Gerber, C. D. Wright, and G. Asti, NATO ASI Ser. E, Applied Sciences (Kluwer, Dordrecht, 1994), Vol. 253.
[9] H. Guerrero, G. Rosa, M. P. Morales, F. del Monte, E. M. Moreno, D. Levy, R. Pérez del Real, T. Belenguer, and C. J. Serna, Appl. Phys. Lett. **71**, 2698 (1997).
[10] G. W. Day and A. H. Rose, Proc. SPIE **985**, 138 (1988).
[11] M. J. Weber, Proc. SPIE **681**, 75 (1986).
[12] G. E. Lano and C. Pinyan, Laser Focus World **31**, 125 (1995).
[13] V. Papaefthymiou, A. Kostikas, A. Simopoulos, D. Niarchos, S. Gangopadyay, G. C. Hadjipanayis, C. M. Sorensen, and K. J. Klabunde, J. Appl. Phys. **67**, 4487 (1990).
[14] F. Chaput, J. P. Boilot, M. Canva, A. Brun, R. Perzynski, and D. Zins, J. Non-Cryst. Solids **160**, 177 (1993).
[15] O. Jarjayes, P. H. Fries, and G. Bidan, J. Magn. Magn. Mater. **137**, 205 (1994).
[16] J. L. Dormann, F. D'Orazio, F. Lucari, E. Tronc, P. Prené, J. P. Jolivet, D. Fiorani, R. Cherkaoui, and M. Noguès, Phys. Rev. B **53**, 14291 (1996), and references therein.
[17] F. Bentivegna, J. Ferré, M. Nyvlt, J. P. Jamet, D. Imhoff, M. Canva, A. Brun, P. Veillet, S. Visnovsky, F. Chaput, and J. P. Boilet, J. Appl. Phys. **83**, 7776 (1998).
[18] Yu. L. Raikher, J. Magn. Magn. Mater. **39**, 11 (1983).
[19] J. C. Bacri, R. Perzynski, D. Salin, V. Cabuil, and R. Massart, J. Magn. Magn. Mater. **62**, 36 (1986).
[20] H. W. Davies and J. P. Llewellyn, J. Phys. D **12**, 1357 (1979).
[21] J. Ferré and G. A. Gehring, Rep. Prog. Phys. **47**, 513 (1984).
[22] M. Nyvlt, Ph.D. thesis, Charles University, Prague, 1996.
[23] O. Cermakova and S. Visnovsky, J. Phys. B **36**, 537 (1986).
[24] M. Abe and M. Gomi, Jpn. J. Appl. Phys., Part 1 **23**, 1580 (1984).
[25] T. K. Xia, P. M. Hui, and D. Stroud, J. Appl. Phys. **67**, 2736 (1990).
[26] J. K. Vassiliou, V. Mehrotra, M. W. Russell, E. P. Giannelis, R. D. Mc Michael, R. D. Shull, and R. F. Ziolo, J. Appl. Phys. **73**, 5109 (1993).
[27] H. Wang, J. Shen, and J. Qian, J. Magn. Magn. Mater. **73**, 103 (1988).
[28] G. B. Scott, D. E. Lacklison, H. I. Ralph, and J. L. Page, Phys. Rev. B **12**, 2562 (1975).
[29] S. Visnovsky, V. Prosser, R. Krishnan, V. Parizek, K. Nitsch, and L. Svobodova, IEEE Trans. Magn. **MAG-17**, 3205 (1981).
[30] S. Visnovsky, Czech. J. Phys., Sect. B **36**, 625 (1986).
[31] J. C. Bacri and D. Gorse, J. Phys. (Paris) **44**, 985 (1983).
[32] H. Takei and S. Chiba, J. Phys. Soc. Jpn. **21**, 1255 (1966).
[33] P. C. Scholten, IEEE Trans. Magn. **11**, 1400 (1975).
[34] J. C. Bacri *et al.* (unpublished).
[35] J. P. Llewellyn, J. Phys. D **16**, 95 (1983), and references therein.
[36] W. J. Tabor and F. S. Chen, J. Appl. Phys. **40**, 2760 (1969).
[37] A. J. Kurtzig, J. Appl. Phys. **42**, 3494 (1971).